Satellite-derived equilibrium shoreline modelling at a high-energy meso-macrotidal beach

Georgios Azorakos, Bruno Castelle, Vincent Marieu, Déborah Idier

Journal Pre-proof

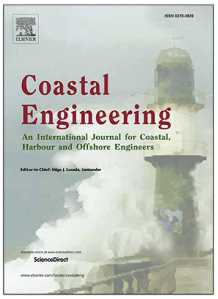

Satellite-derived equilibrium shoreline modelling at a high-energy meso-macrotidal beach

Georgios Azorakos, Bruno Castelle, Vincent Marieu, Déborah Idier

PII: S0378-3839(24)00084-X
DOI: https://doi.org/10.1016/j.coastaleng.2024.104536
Reference: CENG 104536

To appear in: *Coastal Engineering*

Received date : 19 September 2023
Revised date : 29 April 2024
Accepted date : 5 May 2024

Please cite this article as: G. Azorakos, B. Castelle, V. Marieu et al., Satellite-derived equilibrium shoreline modelling at a high-energy meso-macrotidal beach. *Coastal Engineering* (2024), doi: https://doi.org/10.1016/j.coastaleng.2024.104536.

Satellite-derived equilibrium shoreline modelling at a high-energy meso-macrotidal beach

Georgios Azorakos[a], Bruno Castelle[a], Vincent Marieu[a], Déborah Idier[b]

[a] *Univ. Bordeaux, CNRS, Bordeaux INP, EPOC, UMR 5805, Alleé Geoffroy Saint-Hilaire, Pessac, 33615, Nouvelle Acquitaine, France*
[b] *BRGM, (French Geological Survey), 3 Av. Claude Guillemin, Orléans, 45100, Centre, Val de Loire, France*

Abstract

Modelling and predicting the future of sandy shorelines is a key challenge in coastal research and is critical for sustainable coastal management. However, currently the most skillful shoreline models strongly rely on data to calibrate the free parameters, and are thus restricted to a few well monitored sites in the world. Here we address the challenges and opportunities offered by optical satellite imagery to provide useful information for equilibrium shoreline model calibration on cross-shore transport dominated sites. We focus on Truc Vert beach, southwest France, where previous work showed good equilibrium model skill to reproduce shoreline change from the time scales of hours (storms) to decades. Satellite derived waterlines are extracted over 11 years (2009-2020) and further transformed into satellite derived shorelines (SDS) with different water level corrections (e.g. tide and/or run up) and varying alongshore averaging lengths, and thus different uncertainties, in order to test model performance. Successively the timeseries duration and sampling frequency required for model calibration were also investigated. The model calibrated using the SDS data showed similar skill as the model

calibrated using in-situ alongshore averaged shoreline positions, even for the uncorrected SDS dataset which Root Mean Square Error (RMSE) are approximately 30 m. Alongshore averaging was found to be the only necessary processing of the SDS data while any other site-specific corrections did not significantly improve model skill. Finally to further investigate the effect of sampling frequency and noise in the dataset we performed an analysis using a synthetic shoreline. Our results suggest that the effect of noise is negligible as long as the sampling frequency remains high (dt $\leq$ 30 days). Pending further validation, results show the strong potential of using uncorrected SDS dataset for shoreline model calibration at cross-shore transport dominated sandy coasts.

Keywords:

Shoreline, Satellite data, Numerical modelling, Calibration

1. Introduction

Coastal areas constitute some of the most populated and developed land zones in the world (Small and Nichols, 2003) with high natural and socio-economical significance (Ghermandi and Nunes, 2013). Luijendijk et al. (2018) found that $\sim$ 24% of the global ice free sandy shorelines are eroding at rates exceeding 0.5 m/year, while Vousdoukas et al. (2020) suggested that these numbers are projected to increase under the influence of climate change. Although more in depth analysis is needed (Cooper et al., 2020), these findings highlight the importance of monitoring, understanding and predicting sandy shoreline evolution.

Sandy coasts can be highly dynamic environments constantly adjusting

their position in response to a variety of processes spread over a wide spatio-temporal range. Changes in sediment availability and mean sea level influence shoreline response on the timescales ranging from decades to millenia (Larson and Kraus, 1995; Murray, 2007). On shorter timescales and on cross-shore transport dominated sites, shoreline response is often dictated by variations in incident wave conditions from the time scale of single storms to seasonal and interannual variability in the incident wave climate (Castelle and Masselink, 2023). Anthropogenic factors can also have a significant and potentially irreversible impact on the shoreline position (Aagaard et al., 2004; Ranasinghe and Turner, 2006; Ojeda et al., 2008).

Reduced complexity shoreline models, such as Yates et al. (2009); Davidson et al. (2013); Splinter et al. (2014); Vitousek et al. (2017); Robinet et al. (2018); Antolínez et al. (2019); Tran and Barthélemy (2020) to name a few, have enabled the scientific coastal community to successfully simulate sandy shoreline evolution from timescales of days (single storms) to years (seasonal and interannual variability) and even to decades (long term shoreline trends) (Splinter et al., 2013; Castelle et al., 2014; Robinet et al., 2020). Not resolving all the complex processes explicitly reduces the computational cost of these models. While process based models need more data like complete topography and bathymetry of an area, reduced complexity models require mainly shoreline position datasets spanning over several years for their calibration (Montaño et al., 2020). Of particular relevance are equilibrium shoreline models that show very good skill on cross-shore transport dominated sites (Splinter et al., 2014). Splinter et al. (2013) showed that due to the empirical and data driven nature of these equilibrium models, high-quality observa-

tional datasets spanning more than 5 years are needed for the calibration of the free parameters. High-quality observational datasets however are limited to a few surveyed sites (Turner et al., 2016; Ludka et al., 2019; Castelle et al., 2020; Bertin et al., 2022; McCarroll et al., 2023), or video-monitored beaches (Splinter et al., 2014; Pianca et al., 2015; Ibaceta et al., 2020) in the world, thus limiting the application of equilibrium data driven models.

Publicly available satellite imagery, cradled a new approach in remote sensing and provided long term (more than 30 years) high temporal resolution (approximately bi-weekly) shoreline data covering the entire planet (Vos et al., 2019a). However, Vos et al. (2019a, 2023) recognized issues with shoreline detection on satellite images at gently sloping and meso-macrotidal environments, where low tide images must also be discarded due to the presence of complex bar/rip systems. Castelle et al. (2021) showed that satellite derived shorelines (SDS) at a high energy meso-macrotidal coast can deviate by more than 30 m from the surveyed shoreline position and proposed ways to address the issue. While astronomical tide and runup adjustment provides the best correction at Truc Vert in southwest France (Castelle et al., 2021), Konstantinou et al. (2023) showed that optimal water level correction (astronomical tide and/or set-up and/or runup) strongly depends on beach state. Konstantinou et al. (2023) also showed that low image availability due to e.g. areas with high cloud cover can dramatically restrict temporally the type of phenomenon that can be detected (e.g., seasonal/interannual variability). Finally, open SDS datasets are often extracted along single transects, which are spaced by hundreds of metres, and may not be representative of the true shoreline variability on intermediate beaches due to the presence of

alongshore variable features like migrating megacusp embayments. Transect spacing and alongshore averaging are therefore important processing parameters affecting SDS accuracy. These observations question the reliability of uncorrected SDS data in gently sloping, high-energy and meso-macrotidal environments, especially when lacking in-situ derived shoreline data to compare with. To which extent such SDS data can be used to calibrate data driven equilibrium shoreline models is virtually unknown.

Most studies using SDS observations to date, focused on interannual shoreline variability (e.g. Castelle et al., 2022) or long term trends (e.g. Luijendijk et al., 2018), rather than their potential for modelling applications. A handful of studies integrating SDS observations in dynamic shoreline models have emerged recently. Alvarez-Cuesta et al. (2021a,b, 2024) incorporated 30 years of SDS data into a dynamic shoreline modelling system to simulate 40 km of the Mediterranean Spanish coast. Ibaceta et al. (2022) assimilated SDS data into their model in order to track variability in model free parameters while simulating 14 years of shoreline evolution at a microtidal beach on the east coast of Australia. Vitousek et al. (2023) integrated SDS observations into their shoreline model to hindcast 20 years of coastal change over the entire coast of California. Vitousek et al. (2023) demonstrated that model calibration with water level corrected SDS yielded similar skill to model calibration with in- situ observations at a meso tidal beach. However, the influence of the type of water level correction was not addressed, and the uncorrected SDS were not tested in model calibration. Crucially, uncorrected SDS datasets does not require local beach slope, astronomical tide data and breaking wave parameters for further correction, and can be thus generated

at any site globally.

In the present work we investigate the possibility of using SDS datasets to calibrate the state-of-the-art equilibrium shoreline model proposed in Davidson et al. (2013), by testing different water level corrections at the high energy meso-macrotidal beach of Truc Vert, southwest France. 11 years of SDS data were used and a simulated annealing non-linear optimization algorithm (Bertsimas and Tsitsiklis, 1993) was systematically applied to various SDS datasets (different water level corrections, alongshore averaging lengths, duration and sampling frequency) in order to find the best fit model parameters and further address model skill by comparing with field data. The study site, data used and methodology adopted in the present work are detailed in sections 2 and 3. The results are presented and briefly discussed in section 4 while a detailed discussion and the conclusions follow in sections 5 and 6. Pending further validation, the findings of the present study suggest that uncorrected SDS data can potentially be used to calibrate data driven equilibrium shoreline models in high energy meso-macrotidal environments without a priori knowledge of the site.

2. Field site and data

2.1. Truc Vert beach

The coast of Nouvelle Aquitaine in southwest France (Figure 1b) stretches approximately 250 km along a straight, low-lying shoreline backed by high vegetated coastal dunes (Laporte-Fauret et al., 2020) excluding a few small stretches interrupted by coastal resorts (Castelle et al., 2018b). The offshore wave climate is generated in the north Atlantic ocean predominantly

by eastward tracking extra tropical cyclones (Castelle et al., 2020). In the present work the remote beach of Truc Vert (panel a in Figure 1), located approximately 2 km away from the nearest inland car park beach entry, is chosen as a case study. Besides a mechanical profiling of the coastal dune backing the beach that took place in the early 1980s (Robin et al., 2021), the beach has never been nourished, affected by hard structures or by any direct anthropogenic activity.

Truc Vert is a high energy meso-macrotidal double barred open beach backed by tall ($\sim$ 20-25 m above Mean Sea Level) and wide ($\sim$ 250 m) coastal dunes (see Figure 1). Tide is semi-diurnal with an annual mean spring tidal range of $\sim$ 3.7 m and largest tidal range of $\sim$ 5 m. The wave climate is seasonally modulated with monthly average significant wave height $\overline{H_s}$ and peak wave period $\overline{T_p}$ ranging from 1.11 m and 9 s in July, with a dominant west-northwest direction, to 2.4 m and 12.8 s in January with a dominant west direction (Castelle et al., 2017).

The sediment composition primarily consists of medium quartz sand, with a median diameter of $d_{50} \approx 350\ \mu m$. The beach sediment displays substantial variability ranging from 200 μm to 700 μm, associated with a wide range of bedforms such as bar/rip channels, megacusps, cusps, and megaripples (Gallagher et al., 2011). The outer bar is subtidal and modally crescentic, while the inner bar, situated in the intertidal zone, is mostly classified as a transverse bar and rip and during the summer months tends to transition into a low tide terrace (see Figure 1). The average spacing between rips is approximately 400 m for the inner bar and 700 m for the outer bar, although these values can vary considerably over space and time. The presence of rip

channels incising the inner bar leads to significant alongshore variations in beach morphology, with pronounced megacusp embayments (Figure 1 a) in the alignment of the rip channels typically evolving on seasonal timescales. The outer bar on the other hand, can drive larger scale beach variability during severe storms which can persist for several years (Castelle et al., 2020).

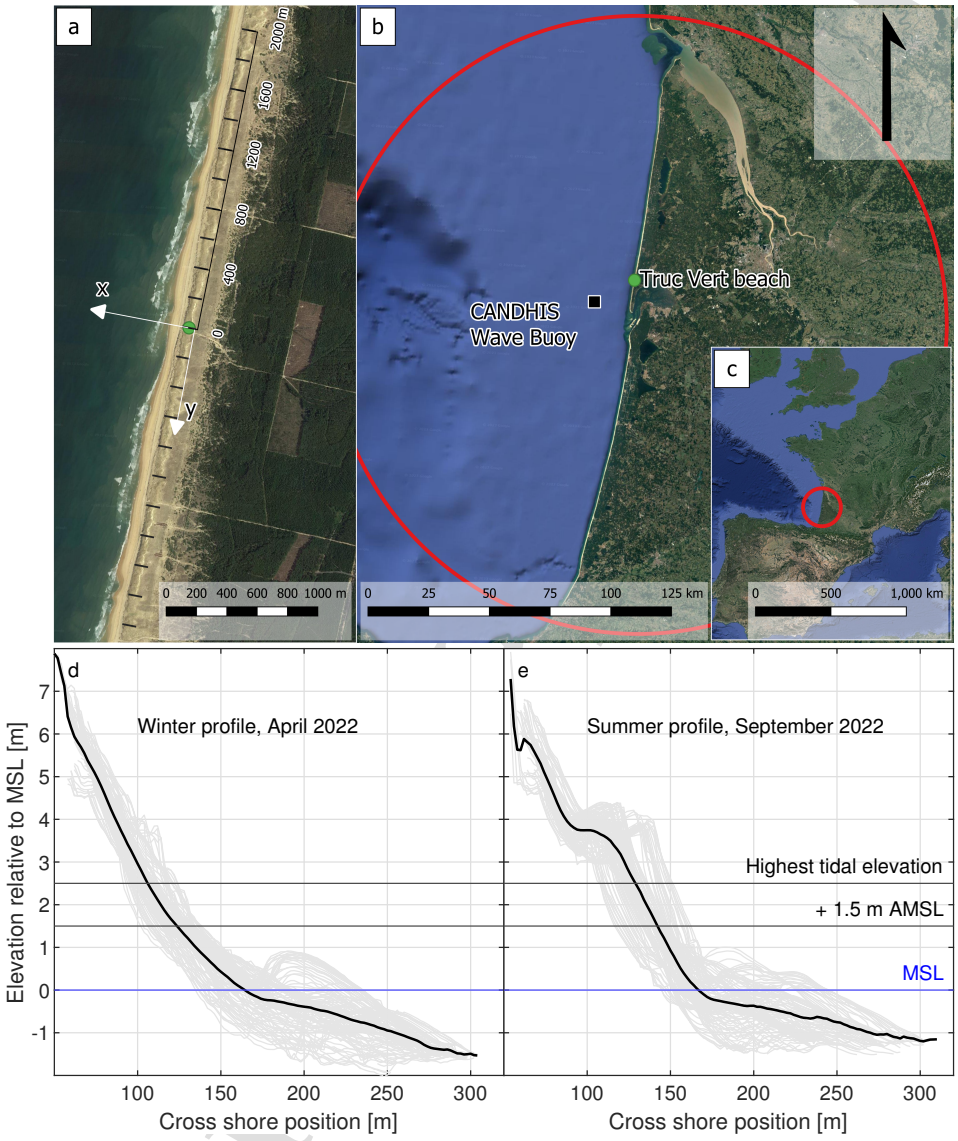

Figure 1: (a) Survey zone and reference frame at Truc Vert beach. (b) Location map of Truc Vert beach, southwest France indicating the position of the CANDHIS wave buoy (Cap Ferret wave buoy 03302). (c) Overview of the area. Winter (d) and summer (e) profiles measured in 2022. The thick black line indicates the alongshore average profile, while the gray lines are the individual profiles extracted every ∼20 m from the alongshore window considered.

In the long term Truc Vert beach can be considered stable (Castelle et al., 2018a), despite the fact that the highly interannually variable winter wave energy can result in severe beach and dune erosion (Castelle et al., 2015; Masselink et al., 2016). The shoreline evolution is mainly dominated by cross shore processes showing strong seasonal and interannual variability, with moderate and extreme winters alternating (Robinet et al., 2016; Masselink et al., 2016).

2.2. Wave Data

Due to lack of continuous wave measurements from the CANDHIS directionnal wave buoy, which is moored in ∼50 m depth offshore of Truc Vert beach (see Figure 1), hourly wave timeseries were extracted from the NORGAS-UG regional wave hindcast (Boudière et al., 2013), at the grid point coinciding with the location of the buoy. The NORGAS-UG regional model covers the Atlantic coast of France on an unstructured mesh. The nearshore is resolved with mesh elements of ∼200 m while the model resolution becomes coarser further offshore with mesh elements of ∼10 km in the deepest parts of the domain.

The wave model results have been validated against several measured data and yielded correlation coefficients of 0.96-0.99, RMSE of 0.15-0.21 m and a bias of -0.02-0.04 m (Michaud et al., 2016). The significant wave height H_s, peak wave period T_p and mean wave direction (MWD) extracted from the aforementioned wave hindcast are depicted in Figure 2. The timeseries shows the typical seasonal and interannual variability of the incident wave climate at Truc Vert beach with a prevailing W-NW wave incidence. The surveyed shoreline is depicted in panel a of Figure 2 together with H_s.

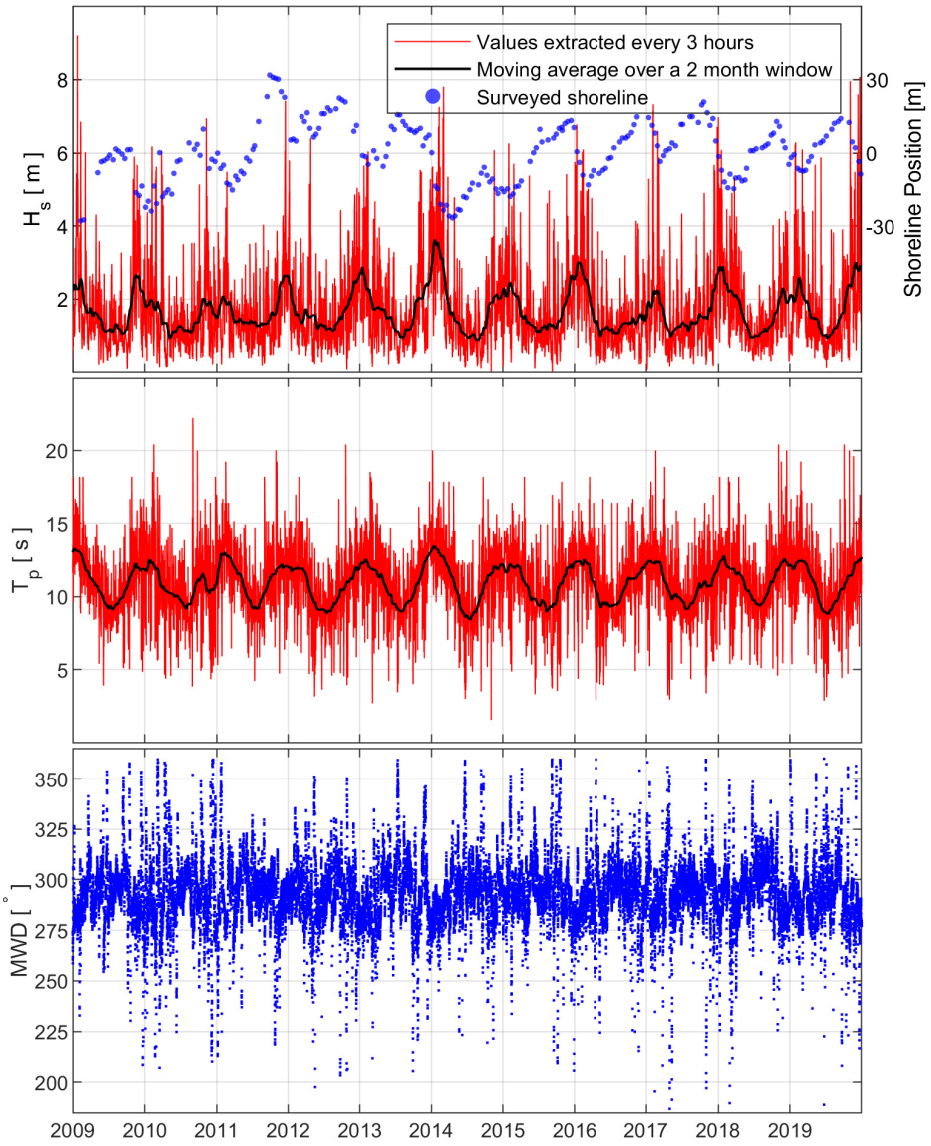

Figure 2: Offshore wave conditions during the period considered in the present work extracted at the location of the buoy (see Figure 1). The significant wave height H_s, peak wave period T_p and mean wave direction (MWD) are depicted in the upper, middle and lower panel of the figure. The alongshore averaged surveyed shoreline positions are plotted on the right axis of the upper panel.

2.3. Shoreline Data

Five different shoreline / waterline datasets extending from January 2009 to December 2019 have been considered in the present work, summarized and depicted in Figure 3. The single transect (S_{IS}) extracted at $y = 0$ (see Figure 1, a) as well as the alongshore averaged in-situ shoreline timeseries ($\overline{S_{IS}}$), have been derived from monthly to bimonthly sampled topographic GNSS surveys, performed during spring low tide at Truc Vert beach (see Figure 1) in the frame of a long-term monitoring program established in 2003 (Castelle et al., 2020). S_{IS} and $\overline{S_{IS}}$ correspond to the 1.5 m elevation Above Mean Sea Level (AMSL) shoreline proxy (see Figure 1), as this has been found to best correlate with the beach-dune volume (Robinet et al., 2016). The overbar denotes alongshore averaging over the survey domain, which increased from approximately 600 m in 2009 to slightly over 2300 m in 2016. In the present work, the alongshore-averaged in situ shoreline $\overline{S_{IS}}$ is considered as the true shoreline to which both satellite-derived and simulated shoreline data will be further compared. Unless stated otherwise the alongshore domain considered in the present work is the largest available at each point in time which after 2016 is stabilized to $\sim$ 2.4 km.

The satellite-derived, alongshore-averaged, uncorrected waterline $\overline{W_S}$, tide-corrected shoreline $\overline{S_{ST}}$ and tide and runup corrected shoreline $\overline{S_{STR}}$ depicted in Figure 3 were generated by Castelle et al. (2021). These datasets were computed from the waterlines W derived from optical satellite imagery along 4 km of coastline at Truc Vert (see panel a in Figure 1). The extraction of the instantaneous waterline position W, was performed using the python toolkit CoastSat (Vos et al., 2019b) which is freely available on GitHub

(`https://github.com/kvos/CoastSat`). CoastSat is a Google Earth Engine enabled open-source Python toolkit that allows the user to obtain waterline position time-series at any sandy coastline worldwide from publicly available satellite imagery. Landsat 5, 7 & 8 (L5, L7 & L8) images with a spatial resolution of 30 m and Sentinel-2 (S2) images with a spatial resolution of 10 m can be retrieved to a user defined window. In succession the images are being processed to remove cloudy pixels and enhance spatial resolution. The methodology for the extraction of the instantaneous waterline position is described in detail in Vos et al. (2019a).

Castelle et al. (2021) applied water level corrections by translating horizontally the waterline W using a constant beach slope of 0.05 and the water level at the coast at the satellite flyover time. The water level at the coast was estimated using a coastal model hindcast of water level (Pineau-Guillou, 2013) validated at Truc Vert by Castelle et al. (2020). To estimate the wave run up component of the instantaneous water level at the satellite flyover time Castelle et al. (2021) used the run up formulations proposed by Senechal et al. (2011) that has been calibrated at Truc Vert and can be scaled using offshore wave height alone at Truc Vert. The two waterline datasets, namely W_S and $\overline{W_S}$ include all usable satellite images since 2009. The two water level corrected datasets $\overline{S_{ST}}$ and $\overline{S_{STR}}$, include all images extracted when total water level η_t exceeds 0.5 & 0.2 m respectively. Although disregarding low tide images improved the quality of the timeseries, it significantly reduces the amount of observations. For a detailed and in depth description of the methodology and analysis resulting to the three satellite derived datasets, the reader is refereed to Castelle et al. (2021).

The raw waterline data extracted from the satellite images W_S as well as its 4-km alongshore averaged dataset $\overline{W_S}$ can deviate from the shoreline position significantly, especially in a high energy meso-macrotidal environment like Truc Vert. The computed root mean square error for the $\overline{W_S}$ dataset reported in Castelle et al. (2021) is in the order of 30 m and the correlation is poor with $R^2 < 0.5$ (see panel c in Figure 3). The single transect satellite derived waterline W_S shows similar agreement when compared against the in situ derived shoreline position S_{IS} considering the same transect (see panel d in Figure 3) with a slightly smaller error. Alongshore averaging and applying tide and/or wave runup correction on the satellite derived waterline positions can largely improve the agreement with in situ shoreline $\overline{S_{IS}}$ (Castelle et al., 2021; Konstantinou et al., 2023). It is important to note that the comparison ($RMSE$, R^2 & $bias$) consider satellite images and beach surveys separated by up to 10 days.

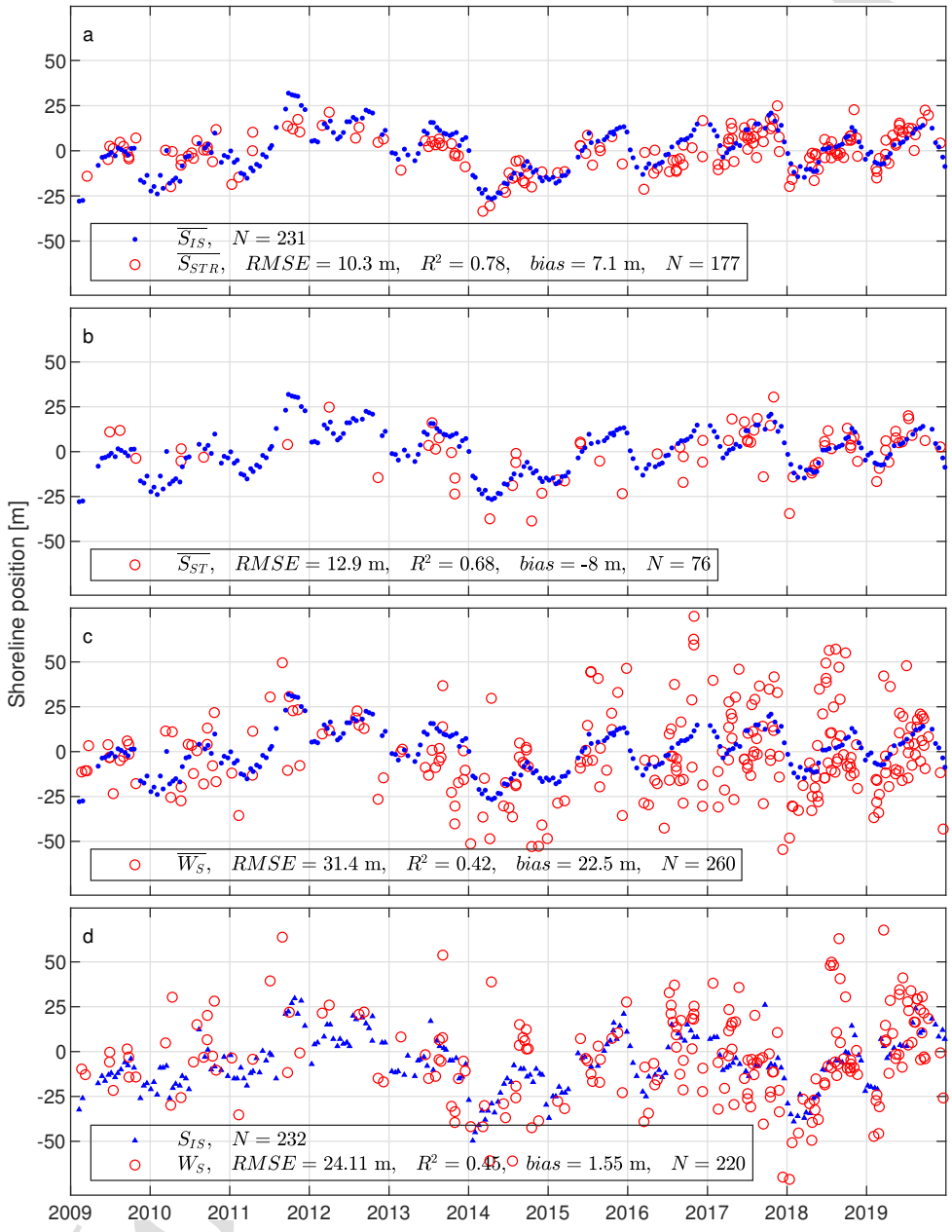

Figure 3: The four different satellite derived shorelines are depicted together with the in situ derived single transect (S_{IS}) and alongshore averaged ($\overline{S_{IS}}$) +1.5 m AMSL shoreline proxy. The $RMSE$, R^2 and $bias$ compared to the $\overline{S_{IS}}$ and S_{IS} as well as the total number of unique observations N for each data set are indicated in the legend.

3. Shoreline numerical modelling

3.1. Equilibrium shoreline model

In the present work the empirical equilibrium shoreline model ShoreFor developed by Davidson et al. (2013) was used to simulate shoreline evolution. In ShoreFor the shoreline displacement is defined as a function of the nearshore wave power and a disequilibrium state of the beach. In the approach of Davidson et al. (2013) the rate of shoreline change dx/dt (m/s) is defined as:

$$\frac{dx}{dt} = c^{\pm} P^{0.5} (\Omega_{eq} - \Omega) \tag{1}$$

where the model's forcing term is the product of the incident wave power P (W) computed using linear wave theory, and the model free parameter $c^{\pm}$ representing the response rate of the shoreline with units of velocity per measure incident wave power. The parameter $c^{\pm}$ is separated into accretion c^{+} when $\Omega_{eq} > \Omega$ and erosion c^{-} when $\Omega_{eq} < \Omega$ components, accounting for the fact that accretion and erosion are observed to evolve at different rates. Davidson et al. (2013) included a term b in their formulation accounting for linear trends stemming from longer term processes that are not explicitly addressed in the model. In the present work this term is disregarded due to the relatively small trend calculated from the SDS data, and the absence of significant shoreline trend over the last 70 years (Castelle et al., 2018b). The term inside the parenthesis in equation 1 is a disequilibrium term which is based on the premise that shoreline state and morphological change are inter-related. Ω is the so called dimensionless fall velocity defined as:

$$\Omega = \frac{H_s}{T_p w_s} \tag{2}$$

where H_s and T_p are the instantaneous significant wave height and peak wave period respectively and w_s is the terminal fall velocity of the beach's median grain diameter d_{50} calculated using Stoke's law. The time varying equilibrium condition Ω_{eq} is a weighted average of the antecedent dimensionless fall velocity Ω defined as:

$$\Omega_{eq} = \sum_{j=0}^{2\phi} \Omega_j 10^{-j/\phi} \left[\sum_{j=0}^{2\phi} 10^{-j/\phi} \right]^{-1} \tag{3}$$

where j is the number of days prior to the present time and the memory decay ϕ is a model free parameter indicating the number of days it takes for the weighting to reach 10%, 1% and 0.1% of the instantaneous value at ϕ, 2ϕ and 3ϕ days prior to the present. The formulation used in the present work and shown in Equation 3 incorporates all past beach state information for the past 2ϕ days, yielding a minimum weighting factor of 1%.

Following the work of D'Anna et al. (2022) a constant SLR_{rate} of 3.31 mm/year is applied, the contribution of which to shoreline retreat is calculated using the Bruun rule (Bruun, 1962). The SLR driven shoreline retreat is negligible in the time scales addressed in the present work.

3.2. Calibration

The model requires the calibration of two model free parameters, namely the accretion/erosion rate $c^{\pm}$ and the memory decay ϕ. An extra term is added allowing the model to adjust its initial position by dx_0. This term is introduced to account for uncertainties in the first shoreline data point.

To calibrate the model free parameters the simulated annealing algorithm proposed by Bertsimas and Tsitsiklis (1993) was implemented. Simulated annealing is a non-linear probabilistic method, that can be used to find the global minimum of a cost function without getting stuck in local minima. The implementation of the simulated annealing algorithm was already successful in the calibration of equilibrium models in Castelle et al. (2014), D'Anna et al. (2020), Labarthe et al. (2023) and more. In this contribution, the mean squared error (MSE) between the observed and simulated shoreline was used as a cost function in the optimization without accounting for any sources of uncertainty.

A timeseries of simulated shoreline evolution and the corresponding cost function C, are calculated based on a set of initial model parameters $\mathbf{P_0}$. Successively, one of the model parameters is randomly selected and modified within the defined range, based on a defined noise. The cost function is calculated for the new set of model parameters $\mathbf{P(i)}$ and compared to the initial value. As long as the new solution is an improvement $C(i) < C$, the same step is repeated with the new solution as initial value $\mathbf{P_0} = \mathbf{P(i)}$ & $C = C(i)$ until the number of iterations defined by the user is reached. In case the new solution is not an improvement $C(i) \geq C$ then the next step is defined based on the following probability:

$$\mathbb{P}(\mathbf{P_0}, \mathbf{P(i)}, T(i)) = \exp[-(C(i) - C)/T(i)]$$

where $T(i)$ is a positive integer called the temperature parameter. The temperature controls the probability of accepting worse solutions. Initially, the temperature is high, allowing the algorithm to accept worse solutions with relatively high probability. The algorithm uses a cooling schedule to gradually

decrease the temperature parameter with every iteration based on a defined cooling coefficient. As the temperature decreases, the algorithm becomes more selective, preferring only better solutions. The temperature parameter plays a crucial role in Simulated Annealing. A high temperature allows the algorithm to explore a wide range of solutions, including worse ones, helping to escape local minima.

The initial model parameters $\mathbf{P_0}$ are defined as the average value of the considered range. The noise amplitude used to inflate each parameter, corresponds to 5% of the bounds' difference. Our preliminary analysis showed that in order to achieve an acceptable solution, the algorithm needed to be initialized with a large temperature T_0, slowly decreasing and allow for a large number of iterations ($O \geq 10^5$).

3.3. Simulation setup

The present work aims to evaluate the performance of the state of the art equilibrium shoreline evolution model proposed by Davidson et al. (2013), when calibrated against satellite-derived waterline and shoreline datasets with different water level corrections and sampling frequencies, and thus varying uncertainties (see Figure 3). To assess the performance of the model and further explore the requirements in SDS quality and quantity to robustly calibrate an equilibrium shoreline model, three different numerical experiments have been designed. All the experiments were conducted under the assumption that there is no a priori knowledge of the simulated coastal environment. This was implemented by investigating a range of calibration parameters (Table 1) beyond the limits found in the literature (e.g. Davidson et al., 2013; Splinter et al., 2014; D'Anna et al., 2020, 2022).

Model parameter	Simulated annealing range	Units
c^+ / c^-	$[0; 2.5] \times 10^{-6}$ / $[0; 1.0] \times 10^{-6}$	$m^{1.5}\ s^{-1}\ W^{0.5}$
ϕ	$[25; 1400]$	days
dx_0	$[-10; 10]$	m

Table 1: Range of values considered in the present work.

As an initial test the model has been calibrated against all five datasets depicted in Figure 3, using the entire period (January 2009 - December 2019) and comparing the model results with the in situ derived shoreline data $\overline{S_{IS}}$ and S_{IS}. This experiment was designed to asses whether the information of the shoreline position can be extracted from the different datasets and to which extent each of the five datasets can be used to calibrate the empirical equilibrium shoreline model and provide accurate hindcast.

Given the alongshore variability in shoreline position due to prominent megacusp embayments, the next experiment was designed to investigate a minimum threshold in the alongshore averaging window necessary to obtain satisfactory model results. To do so, 40 different shoreline datasets were generated from the satellite-derived waterlines W using alongshore averaging windows extending from 100 m to 4000 m around the origo point (see Figure 1), in increments of 100 m. All of these alongshore averaged datasets were used to calibrate the model against the entire period (January 2009 - December 2019). Model performance was systematically assessed against in situ derived shoreline data $\overline{S_{IS}}(y)$ after 2016, using the same window as the calibration dataset. The variable y represents the alongshore distance considered for each window (see Figure 1). Importantly, in order to avoid

erroneous interpretations of the results, account for the stochastic nature of the simulated annealing algorithm and ensure repeatability, the calibration was run 20 times for every dataset.

The final numerical experiments were designed to explore the amount and quality of data required to obtain fair model skill. These experiments were inspired by the work of Splinter et al. (2013), where they investigated the influence of noise, morphological sampling interval and calibration duration in empirical equilibrium shoreline models including Davidson et al. (2013). Similar to the work of Splinter et al. (2013) and more recently Alvarez-Cuesta et al. (2024), in order to properly investigate the influence of sampling frequency as well as noise in the dataset, a synthetic shoreline was generated S_{SYN} using Eq. 1 and the wave timeseries depicted in Figure 2. Subsequently the synthetic shoreline was inflated by normally distributed noise with a magnitude, equal to 100% and 200% of the standard deviation of the synthetic shoreline timeseries to account for measurement errors and other unresolved processes. Finally the synthetic shoreline timeseries were subsampled in intervals of $dt = 1, 7, 14, 30, 60, 90, 182$ & 365 days. The resulting 24 synthetic shoreline timeseries were used to calibrate the model, which performance was evaluated against the daily subsampled synthetic shoreline with 0% noise. The duration of an adequate calibration period was investigated in increments of 6 months for all aforementioned synthetic shorelines as well as the four observed alongshore averaged shoreline timeseries depicted in Figure 3. The performance of the models calibrated using the alongshore averaged shoreline and waterline data was evaluated against the true shoreline ($\overline{S_{IS}}$) timeseries of the subsequent period. All simulations for both the synthetic

and observed datasets, were repeated 10 times to account for the stochastic nature of the simulated annealing algorithm.

Lastly the importance of sampling frequency was further investigated using the alongshore averaged uncorrected waterline data $\overline{W_S}$ over the entire period from January 2009 to December 2019. In this experiment, N amount of data points were randomly sampled from the entire dataset which were then used to calibrate the model over the entire period. Successively the model's performance was evaluated against the true shoreline ($\overline{S_{IS}}$). Eleven datasets were investigated in total with the most scarce one being populated by $N = 25$ points randomly distributed over the entire period and increasing the amount of points in increments of 25 arriving at the complete dataset. The experiment was repeated 30 times for each dataset.

4. Results

4.1. Model calibration with different datasets

Figure 4 shows model results when calibrated with each of the five datasets (namely $\overline{S_{IS}}$, $\overline{S_{STR}}$, $\overline{S_{ST}}$, $\overline{W_S}$ and W_S), which are compared against the in-situ shoreline proxies $\overline{S_{IS}}$ and S_{IS}. For all five datasets, the model was calibrated using the entire period depicted in Figure 4. All the alongshore averaged datasets, both in-situ and satellite derived, produce an acceptable model with RMSE < 10 m and $R^2 \approx 0.6$ (Figure 4). This is not surprising for in-situ shoreline proxy $\overline{S_{IS}}$, with model skill similar to previous equilibrium model applications at Truc Vert (Castelle et al., 2014; Splinter et al., 2014; D'Anna et al., 2020). More unexpected is that similar model skill is obtained with all the alongshore-averaged SDS despite the error and noise

in the dataset (see Figure 3). This is particularly true for the uncorrected waterline $\overline{W_S}$, with RMSE of approximately 30 m and seasonal and interannual patterns barely depictable (Figure 3). Results improve as uncertainties are reduced with each applied correction (tide and/or runup correction), despite the fact that both these datasets contain less data points (Figure 3). In contrast, the model calibrated with the single transect waterline dataset W_S (Figure 4e) shows very poor performance with a coefficient of determination of $R^2 \approx 0.2$ and a RMSE > 10 m, which will be discussed later in the paper.

Given that only the single transect dataset yielded poor results, the influence of alongshore averaging window on model skill was investigated (Figure 5). Results show that the minimum window width to obtain good model skill is $L \geq 1.2$ km. Both the RMSE of the model and the correlation coefficient improve significantly with $L \geq 1.2$ km, while a slight further improvement is observed when $L \geq 2.2$ km. These values coincide with approximately 1.5 and 3 times the wavelength of the megacusp embayments (~ 700 m) observed in Truc Vert beach. It should be noted that the in situ data are limited to a window of ~ 2.4 km. Thus, beyond this point the calibration results have been compared against alongshore averaged shoreline positions using the largest available window (~ 2.4 km). The findings of this experiment are discussed in detail in Section 5.

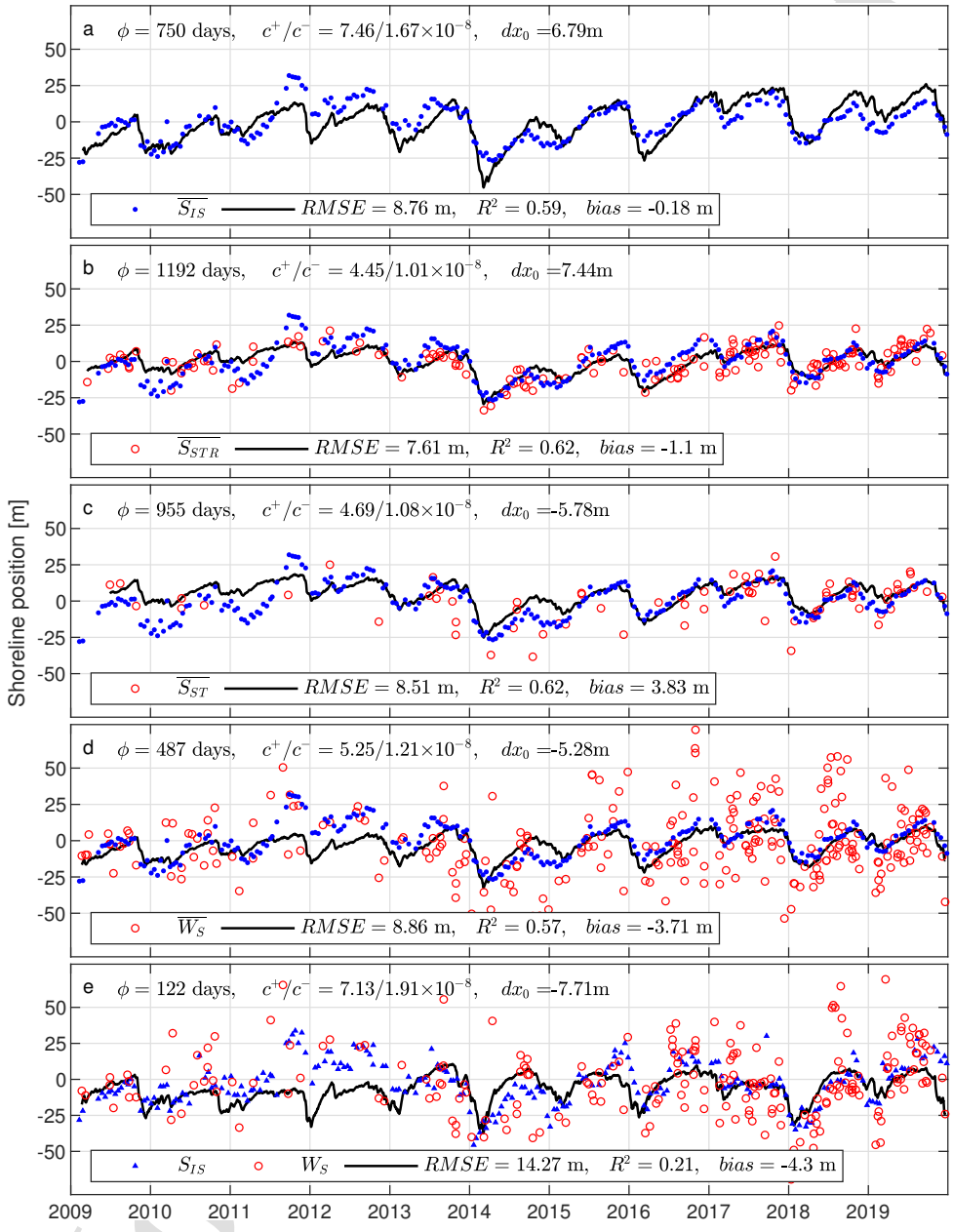

Figure 4: Model results using the simulating annealing algorithm to calibrate the model over the entire period based on the five different datasets and comparing with the in-situ derived shoreline data $\overline{S_{IS}}$ (blue dots) and S_{IS} (blue triangles). Performance metrics and calibrated model parameters are indicated in each panel.

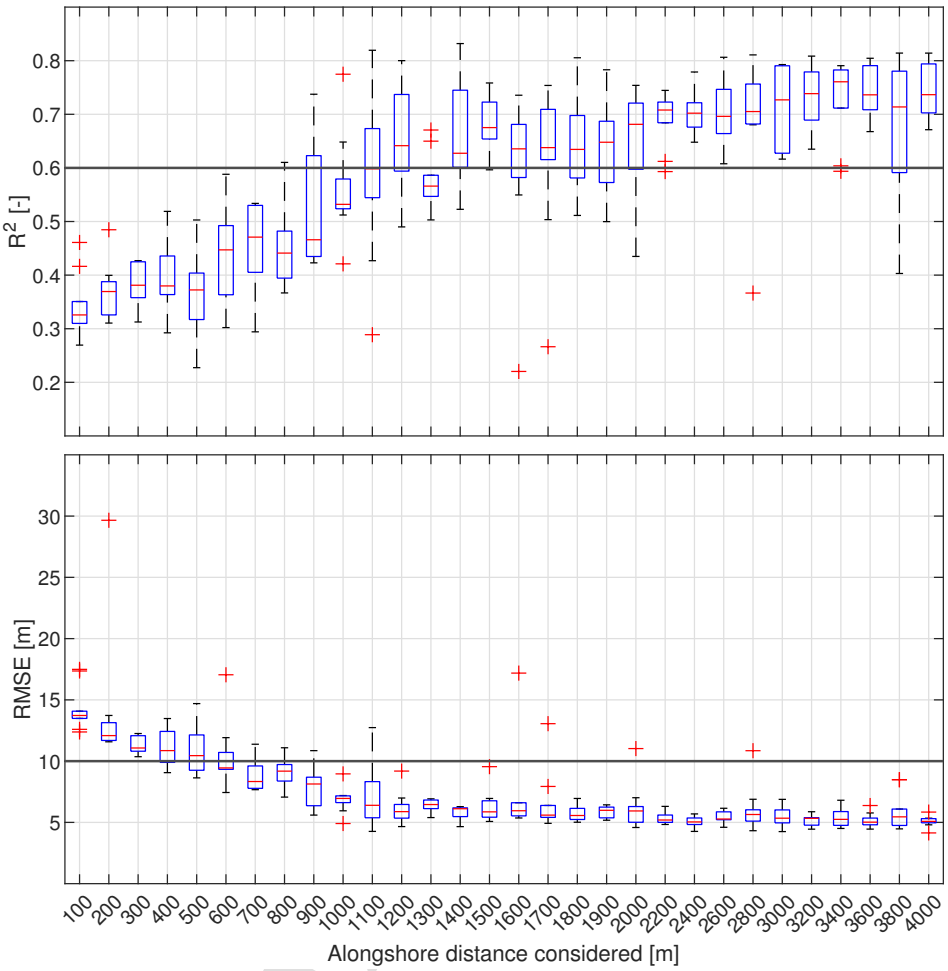

Figure 5: Performance indicators ($RMSE$ and R^2) of the model when calibrated using the alongshore averaged satellite derived waterline ($\overline{W_S}$) with a varying alongshore window size. The performance indicators of the model results are calculated against in-situ shoreline data with a matching window size ($\overline{S_{IS}}(y)$). Each box summarizes the results of 10 calibration runs. The horizontal red line inside the box, indicates the median value and the top and bottom edges of the blue boxes indicate the 25th and 75th percentiles respectively. Maximum whisker length extends up to 1.5 times the interquantile range and any value outside this range is considered an outlier and depicted as a red cross.

4.2. How much data is enough ?

In Figures 6 and 7 the results of the investigation on the adequate calibration period, influence of noise and sampling frequency on model performance using a synthetic shoreline are summarized for the case of 0 % and 200 % noise respectively. The sampling frequency of the shoreline used for calibration is indicated in the upper right corner of each panel. The mean (squares) and standard deviation (circles) R^2 and $RMSE$ of the 10 simulation ensemble are plotted in the left and right hand column respectively.

The influence of sampling frequency is weak in the 0 % noise case for dt $\leq$ 90 days (see Figure 6). Further reducing sampling frequency significantly reduces model skill, especially when less than 4 years of data are used for calibration. Considering a calibration period of 4 years or more, all four datasets enable the generation of models with very similar skill. The larger $RMSE$ around the 5 year calibration duration is due to the model producing an erroneous trend.

The effect of noise in the dataset on model skill is almost negligible as long as the sampling frequency is kept within dt $\leq$ 30 days (see Figures 6 and 7). Reducing sampling frequency to dt $\geq$ 90 days in the dataset with 200 % noise significantly reduces model skill, however when a calibration period larger than 3 years is considered results improve. Further reducing the sampling frequency to dt = 365 days, yields a model that fails to reproduce the shoreline evolution. When calibrating over 4 years or more, the model manages to capture the shoreline variability while still fails to reproduce the shoreline trend. These findings are very promising and are discussed in detail in Section 5.

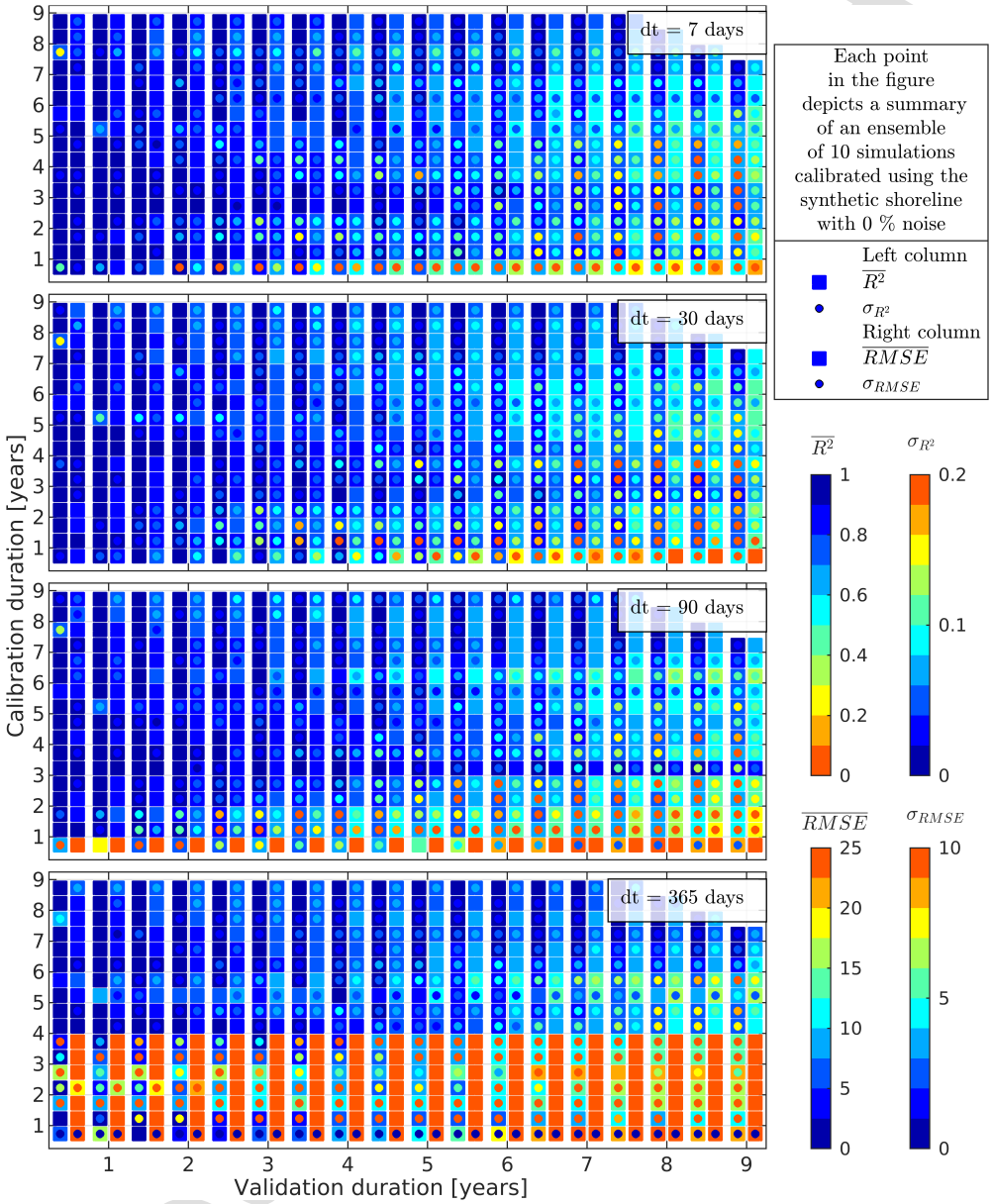

Figure 6: Model performance calibrated using synthetic shoreline with 0 % noise subsampled at dt = 7, 30, 90 and 365 days. $RMSE$ and R^2 plotted in the left and right column respectively, are calculated based on the daily subsampled synthetic shoreline considering the period following the calibration.. The squares and the circles represent the mean and standard deviation of an ensemble of 10 simulations.

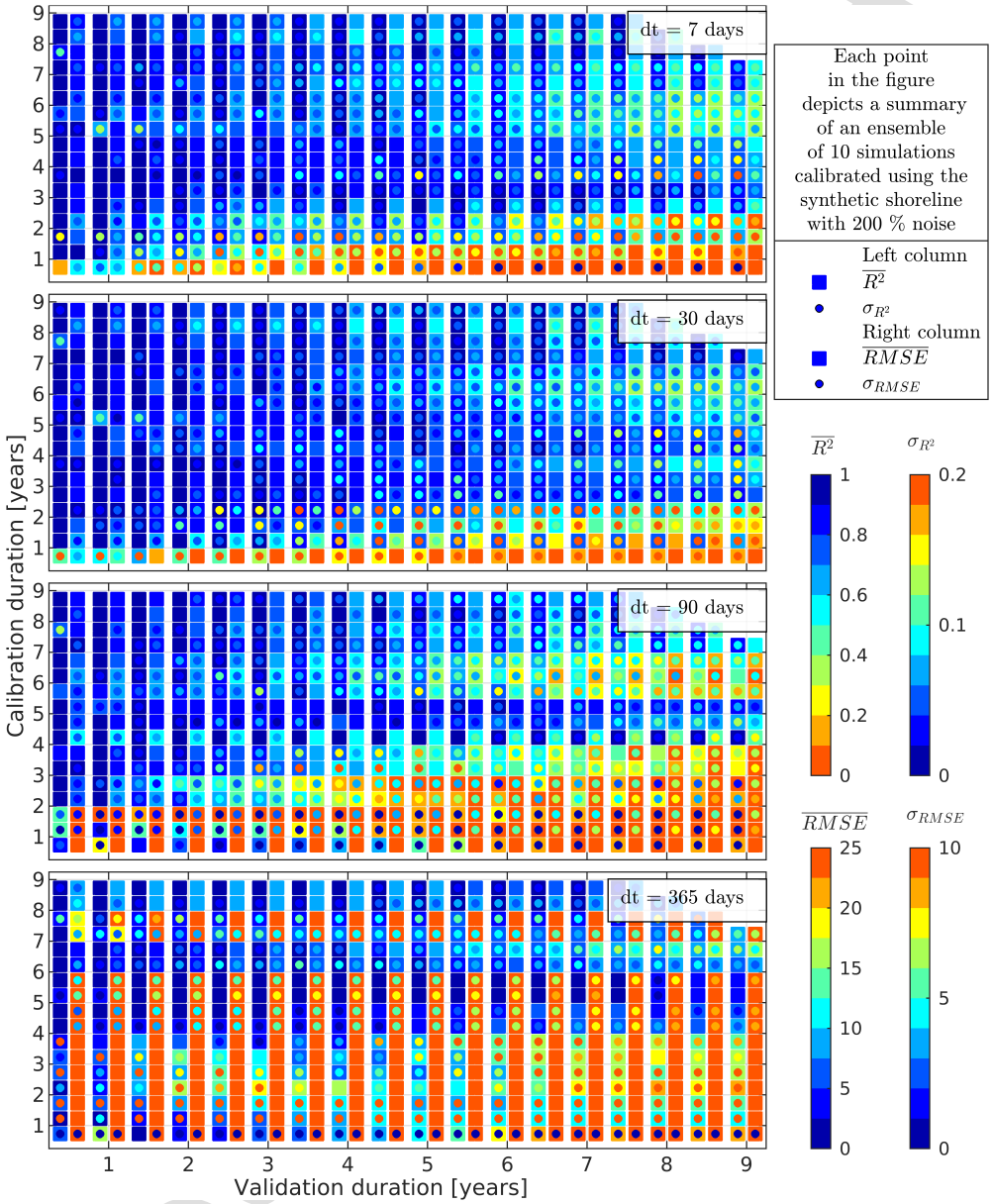

Figure 7: Model performance calibrated using synthetic shoreline with 200 % noise subsampled at dt = 7, 30, 90 and 365 days. $RMSE$ and R^2 plotted in the left and right column respectively, are calculated based on the daily subsampled synthetic shoreline considering the period following the calibration.. The squares and the circles represent the mean and standard deviation of an ensemble of 10 simulations.

In Figure 8 the predicted shorelines from the investigation on the adequate calibration period using the four alongshore averaged datasets are depicted together with the dataset used for the calibration. In Figure 9 the results of the analysis are depicted in the same format as for the synthetic cases. Results for all datasets, indicate a pivot point in model skill when calibration duration exceeds 4 years. This finding agrees with the work of Splinter et al. (2014) and our tests on the synthetic shoreline dataset. Excluding the $\overline{S_{ST}}$ dataset the models produced considering a calibration period of 4 years or more, show very good model skill. The increase in $RMSE$ in the model calibrated with the $\overline{W_s}$ considering a 6 year period is attributed to an erroneous trend generated by the model. This trend is present in the $\overline{W_s}$ dataset between 2009 and 2015, leading to model parameters that would reproduce it. These findings open new perspectives for SDS applications which are discussed in more detail in Section 5.

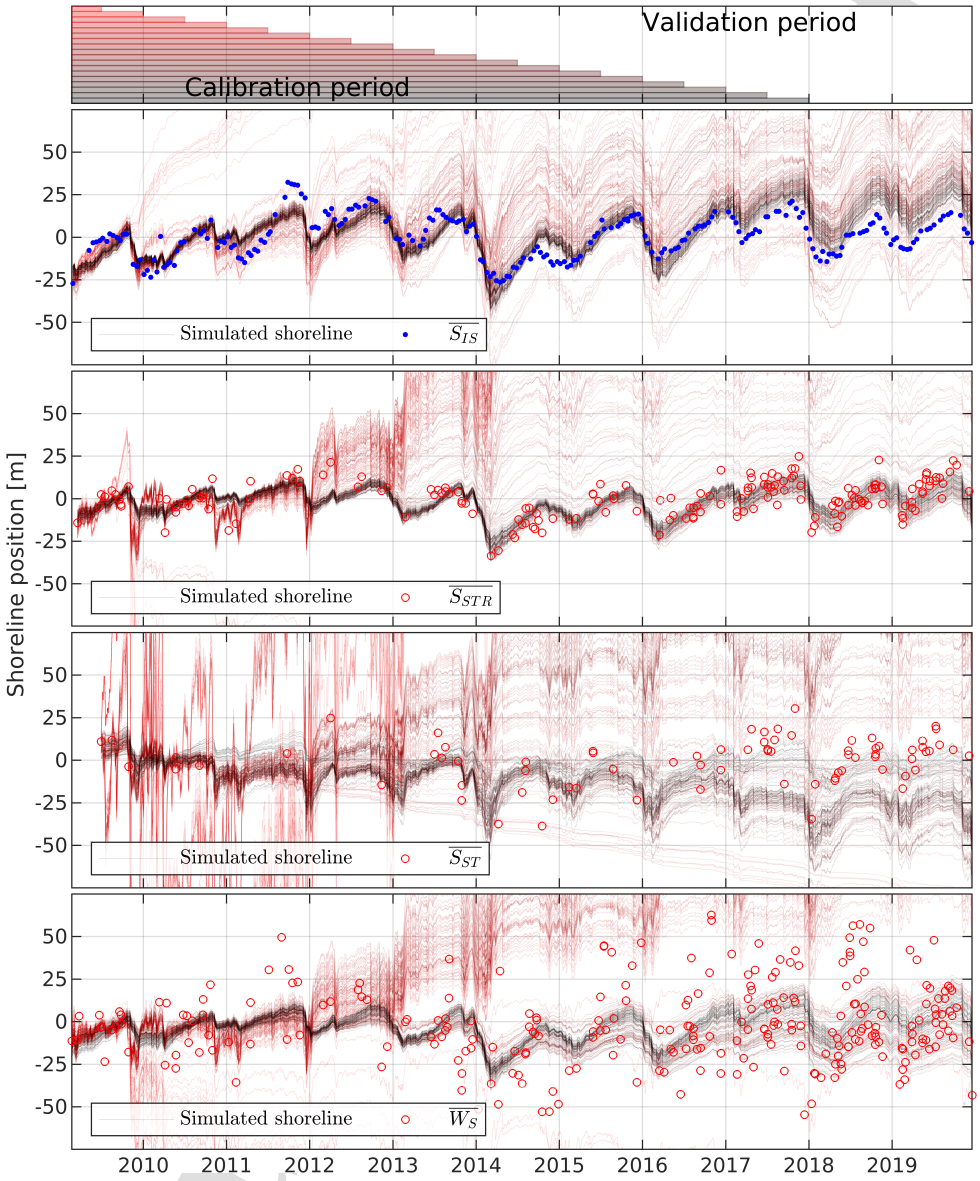

Figure 8: Model results of the investigation on the sufficient calibration window for all four alongshore averaged datasets. The considered calibration periods are indicated in the upper panel The considered calibration periods are indicated in the upper panel, transitioning from red to black as the calibration duration increases. The simulated shorelines are plotted in red for the model calibration finishing at 07/2009 gradually transitioning to black as the calibration window increases. Model performance was evaluated against the $\overline{S_{IS}}$ dataset considering the period following the calibration.

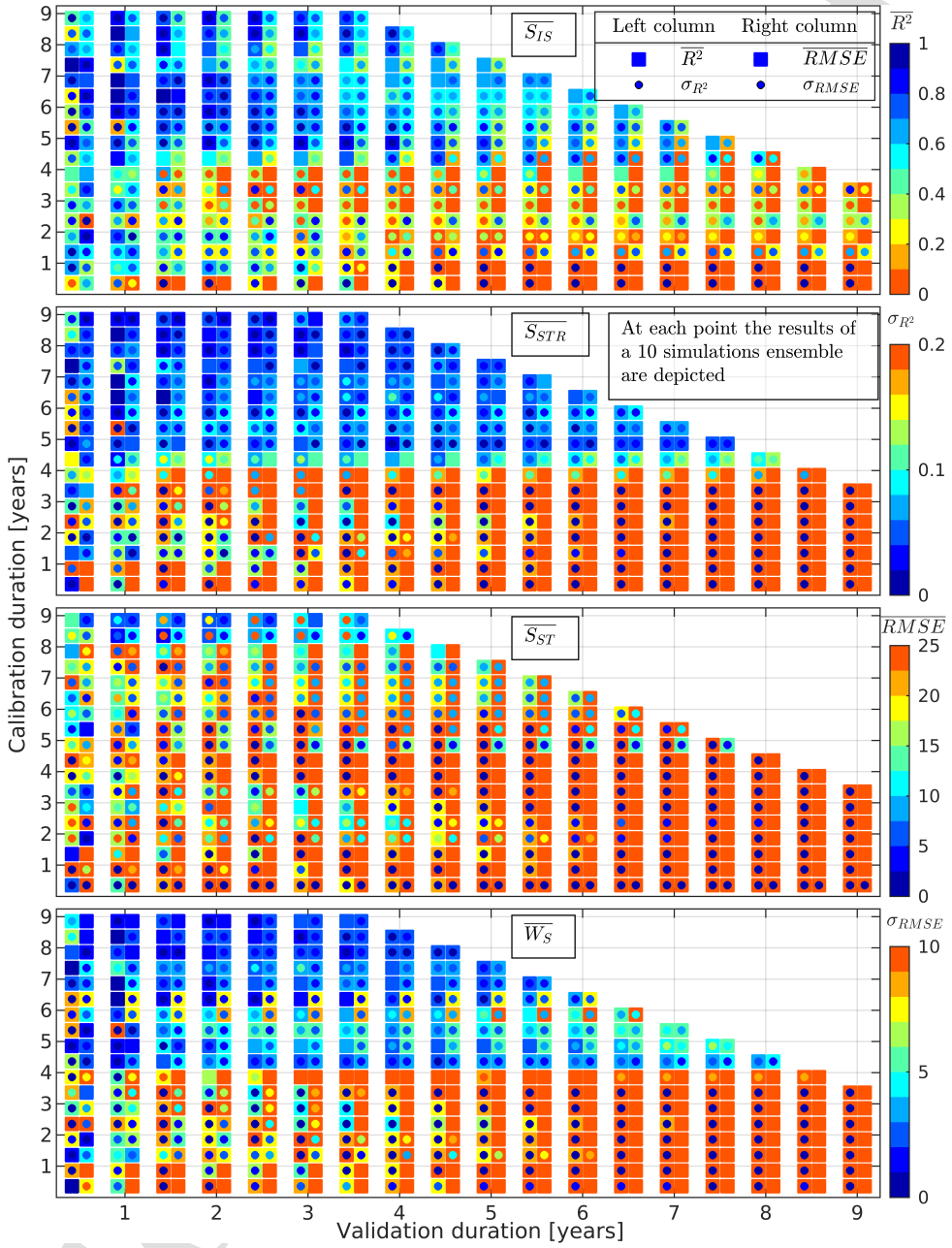

Figure 9: Model performance calibrated using the four alongshore averaged observed datasets, evaluated against the $\overline{S_{IS}}$ dataset considering the period following the calibration. $RMSE$ and R^2 plotted in the left and right column respectively. The squares and the circles represent the mean and standard deviation of an ensemble of 10 simulations.

Finally the results on the influence of sampling frequency in the alongshore averaged uncorrected SD waterline $\overline{W_S}$ on model skill are depicted in Figures 10 and 11. In Figure 10 four examples are shown having a total number of observations over the entire 11 year period of N = 25, 100, 175 and 275 plotted from the upper to the lower panel, respectively. The results are summarised in Figure 11 in terms of performance metrics ($RMSE$ and R^2). These findings indicate that even with a dataset of 25 points distributed randomly over the 11 year period the simulated annealing algorithm manages to find an acceptable solution. However, the majority of the runs based on calibration with only 25 points yield very poor results. Increasing the number of points shows a significant improvement in the repeatability of the solution. When using the complete dataset (N_{max} = 275 points), the algorithm never fails to find an acceptable solution. These results are discussed in detail in section 5.

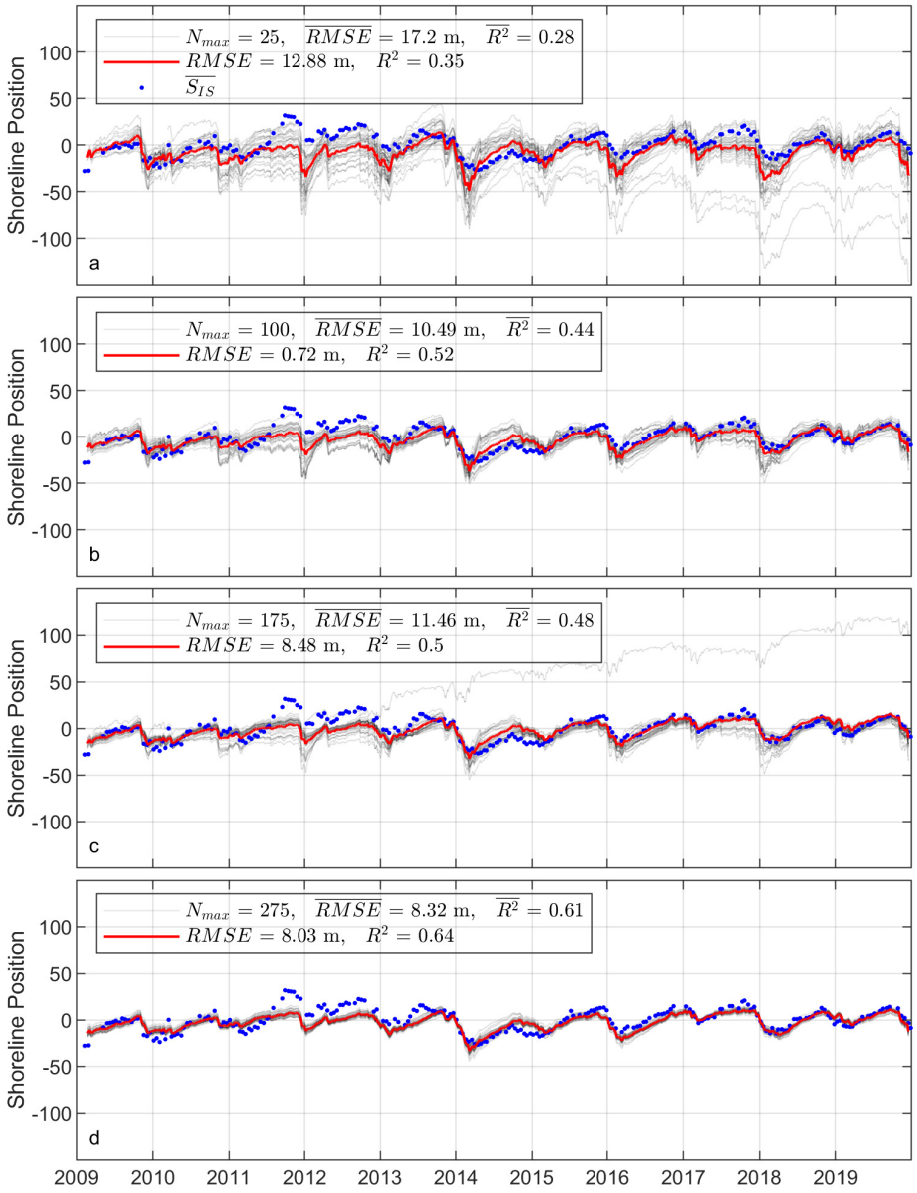

Figure 10: Predicted shoreline obtained from an ensemble of 30 different model calibrations using N number of randomly selected points from the $\overline{W_S}$ data set. The ensemble mean is plotted in red while all the rest are plotted in light grey. The model's performance is evaluated against the $\overline{S_{IS}}$ (blue dots). The amount of data points N_{max} used for the calibration of the model is indicated in the legend together with the average performance indicators $\overline{RMSE}$ and $\overline{R^2}$ of the ensemble.

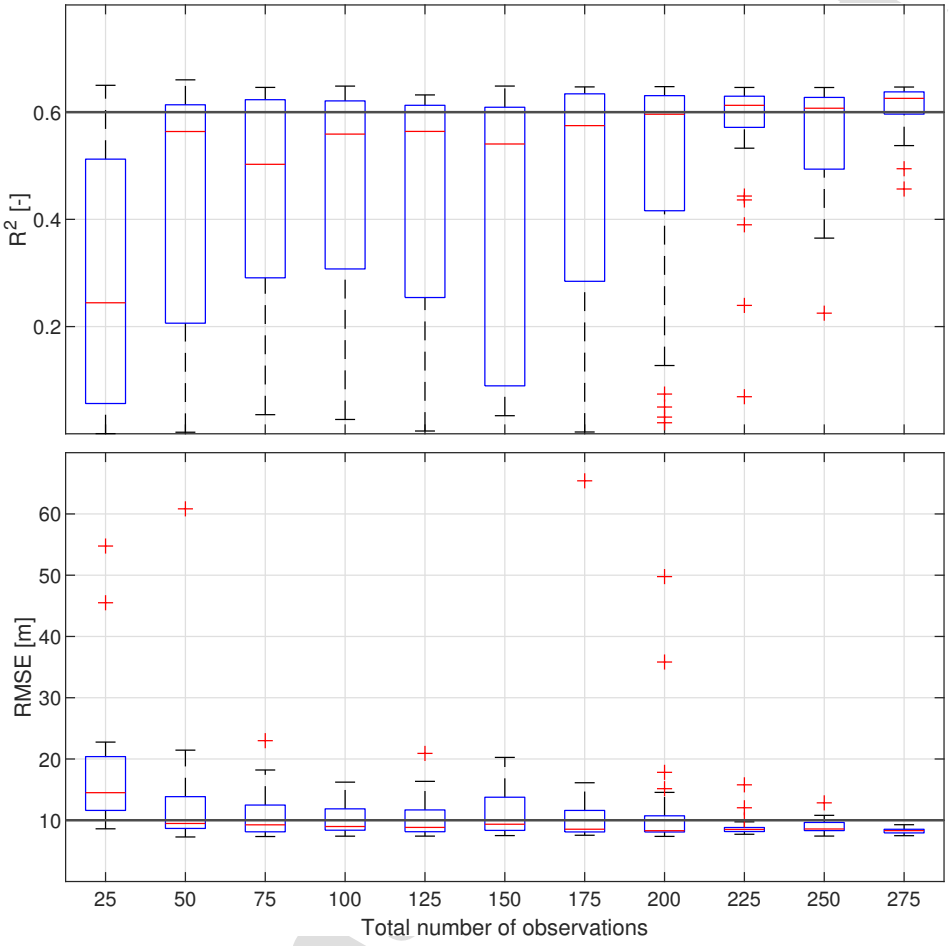

Figure 11: Performance indicators $RMSE$ and R^2 depicted in the lower and upper panel of the figure plotted against the number of data points used for the calibration. Each box corresponds to an ensemble of 30 simulations using N amount of data points randomly selected from the $\overline{W_S}$ dataset. The horizontal red line inside the boxes, indicates the median value and the top and bottom edges of the blue boxes indicate the 25th and 75th percentiles respectively. Maximum whisker length extends up to 1.5 times the interquantile range and any value outside this range is considered an outlier and depicted as a red cross.

5. Discussion

To the authors' knowledge the current study is the first ever successful use of uncorrected SDS data for the calibration of an equilibrium shoreline model in a high-energy, meso- macrotidal environment. Previous studies such as Castelle et al. (2014); Splinter et al. (2014) have used either data collected using traditional survey techniques such as GNSS or video-derived shorelines (e.g. Holman et al., 2003, ARGUS). Existing work using SDS observations in model calibration focused on microtidal environments (e.g. Alvarez-Cuesta et al., 2021a,b; Ibaceta et al., 2022), where SDS RMSE are in the order of 10 m. In their latest contribution Vitousek et al. (2023) applied a SDS data assimilated shoreline model to hindcast and predict coastal change at the entire coast of California. They used almost exclusively SDS data for the calibration of the model, to which they applied water level corrections achieving a RMSE between SDS and in situ observations in the order of 15 m.

There is a substantial amount of research aiming at reducing uncertainties and improve quality of SDS data (Castelle et al., 2021; Konstantinou et al., 2023). In the present application however the amount of data was found to be the most important parameter of the SDS dataset rather than the quality/accuracy of the shoreline position. Without applying any of the corrections proposed in Castelle et al. (2021), SDS data extracted in a meso-macrotidal, high-energy environment with a RMSE larger than 30 m, allowed skillful equilibrium shoreline model calibration. The calibrated model showed a very good performance with a RMSE = 8.3 m and a strong correlation of R^2 = 0.63. This result was unexpected considering the large RMSE associated

with the raw SDS data.

The effect of noise in the datasets (both synthetic and observed) seems to be almost negligible as long as the sampling frequency is kept high (dt $\leq$ 30 days) and an adequate calibration period is considered. This observation stemming from the synthetic shoreline analysis experiment clearly explains why the worst model skill is obtained when the tide corrected dataset $\overline{S_{ST}}$ is used for calibration. The model seems to be sensitive to the period chosen for calibration as this would influence the shoreline trend as well as the phenomena included. Further analysis considering different calibration periods while maintaining the same duration should be performed to investigate this hypothesis.

It should be stated that the in situ data include a strong accretion spike in 2012 which is due to sandbar-welding and could only be captured at spring low tide which is when surveys take place at Truc Vert. This accretion signal is not as pronounced in the SDS datasets since the satellite flyover time does not necessarily coincide with spring low tide. Furthermore, as previously discussed the water level corrected datasets disregard low tide images, which results in smoothing of the accretion spike. Such an event could not be captured by the physics of the model used, and is believed to have an impact in the performance of the model when calibrated with this period of the in-situ dataset. This could also be partly the reason for increasing model performance as the influence of 2012 gets smoothed with larger calibration period (see Figure 9).

The fact that the adopted methodology proved successful even in a very challenging site such as Truc Vert, is very encouraging for potential future

applications of SDS data in equilibrium shoreline modelling even at sites where no in-situ data are available. The spatio-temporal coverage of freely available satellite imagery combined with the no a priori knowledge assumption adopted in the current study, hint that the proposed methodology could be universally applicable on cross-shore transport dominated coasts. The model used in the present work requires information about the median sediment grain size D_{50} of the simulated environment. Although this information is impossible to obtain via remote sensing, a reasonable guess would be sufficient as this would serve as a scaling factor that would be compensated by the calibration parameters.

Alongshore averaging was found to be the only necessary processing of the SDS data prior to their application in model calibration at Truc Vert. This can be explained by the presence of prominent mega-cusps, that typically form, migrate alongshore, and decay in time, which physics are not represented by an equilibrium model like Davidson et al. (2013). Therefore these features needed to be filtered out of the dataset, which was achieved by alongshore averaging over a window approximately 1.5 times the features wavelength. This approach does not violate the no a priori knowledge assumption adopted, since megacusp spacing can be estimated by simply studying the satellite images, and an averaging window of say 3-4 time this spacing be applied. Alternatively, filtering out megacusps, which are quite common on intermediate coastlines (Wright and Short, 1984), can be performed by applying a conservative alongshore window width in the order of a couple of km as Truc Vert shows larger rip spacing than most of the reported sandy beaches. Critically, our findings are in line with recent work suggesting that

spacial averaging can reduce SDS noise (Castelle et al., 2022; Warrick et al., 2023), and demonstrate that global SDS datasets with transects spaced by 10s of kilometers are not relevant to address shoreline change on most coasts (Warrick et al., submitted).

A dataset covering 4 to 5 years with a monthly sampling frequency was found to be sufficient for the calibration of the model applied to hindcast ∼6 years of shoreline evolution in Truc Vert. This result, obtained with raw SDS data in a high energy, meso- macrotidal shoreline, is in line with the findings of Splinter et al. (2013) where they investigated the influence of noise, morphological sampling interval and dataset duration in equilibrium shoreline model calibration and the recent work of Alvarez-Cuesta et al. (2024) who performed a similar analysis on data assimilation. The fact that similar results with previous studies are obtained in the present work, further illustrates the strength of the simulated annealing algorithm considering that the investigated noise level in the synthetic time series is 4 times larger compared to previous studies (200% of the standard deviation) and so is the order of magnitude of the observation error ($O \sim 30$ m). It should be noted that the SDS data after 2013, improve both in terms of image quality and sampling frequency. Therefore, the aforementioned result can be considered conservative and the models obtained using the methodology presented in this work are only expected to improve.

Our findings regarding the adequate sampling frequency indicate that even with as few as 25 points randomly spread over an 11 year period, the simulated annealing algorithm was able to find a very good solution. This is particularly encouraging for applications in higher latitudes where the amount

of cloud-free satellite images are significantly reduced (Konstantinou et al., 2023). On average however, the performance of the models calibrated with the scarcely populated datasets ($N_{max} \leq 200$) is considered poor. Results could be significantly improved for all datasets by narrowing the range of investigated model free parameters which would guide the algorithm towards a desired solution.

The alongshore averaging window width and adequate spatiotemporal resolution of the SDS data, should be regarded as site specific variables. Given that Truc Vert is a challenging coastline, conservative estimates of these variables are provided in the current work. Exception would be high-latitude coastlines where cloud coverage can significantly affect the sampling frequency. The limited availability of cloud free satellite images that would significantly affect the temporal resolution could be addressed through an iterative approach. In addition larger waves associated with higher latitudes would influence the size of cusps and megacusps which in turn would control the width and spatial resolution of the alongshore window. The sufficient width and resolution of the alongshore window are not seen as limitations but rather as site-specific information readily available in the satellite imagery.

The present results suggest that the introduced methodology could be potentially applicable to any cross shore dominated sandy shoreline. To verify this hypothesis such approach should be applied to several diverse sites around the world investigating the influence of beach type, wave climate and tidal amplitude in model skill. Furthermore, applying such method to complex coasts where other processes (e.g. longshore sediment transport gradients) are at play should also be explored using one-line models. Finally

applying the same approach to different model types would further challenge the findings of the present study. Although previous work using several models like Yates et al. (2009); Splinter et al. (2014); Vitousek et al. (2017); D'Anna et al. (2022) suggest similar performance, further validation of the proposed methodology should be conducted.

The simulated annealing algorithm has proven to be a very useful tool, enabling the proposed methodology. The stochastic nature of the algorithm should be accounted for by repeating the experiment enough times such as to achieve convergence of the error statistics. Any application of the introduced methodology would require accurate inshore wave data (hindcast and /or forecast), that capture the wave climate variability (e.g. seasonal, interannual). Such data may be obtained from publicly available global wave hindcasts spanning over several decades such as Mentaschi et al. (2023); Hersbach et al. (2023), and either used directly as a forcing or as a boundary condition to produce high resolution nearshore wave forcing for shoreline modelling.

6. Conclusion

The present work introduces a novel approach using uncorrected, noisy, SDS data for the calibration of equilibrium based shoreline models. The simulated annealing algorithm proposed by Bertsimas and Tsitsiklis (1993) guided by high quality wave forcing, extracts information from uncorrected noisy SDS data, even when assuming no a priori knowledge of the site. Rather than data quality, the amount of data (e.g sampling frequency) was found to be critical in the modelling application. The only required processing of the

SDS data for the model calibration was alongshore averaging, while any other site-specific corrections did not significantly improve model skill. Though further validation is needed, our findings suggest that alongshore averaged uncorrected SDS extracted at any cross shore dominated coastline can be applied in the calibration of transect based equilibrium shoreline models. The present work opens new perspectives in modelling, understanding and predicting sandy shoreline change in sites lacking field data.

7. Acknowledgements

This work was done in the framework of the SHORMOSAT project and funded by Agence Nationale de la Recherche (ANR) grant number ANR-21-CE01-0015. This study includes the monitoring site of Truc Vert labelled by the Service National d'Observation (SNO) Dynalit (https://www.dynalit.fr). The Observatoire de la Côte de Nouvelle-Aquitaine (OCNA) and Observatoire Aquitain des Sciences de l'Univers (OASU) provide additional financial support for the surveys. We thank Stéphane Bujan for performing the Truc Vert beach field surveys. NORGAS-UG wave hindcast data was provided by LOPS-Ifremer.

References

Aagaard, T., Davidson-Arnott, R., Greenwood, B., Nielsen, J., 2004. Sediment supply from shoreface to dunes: Linking sediment transport measurements and long-term morphological evolution. Geomorphology 60, 205–224. doi:10.1016/j.geomorph.2003.08.002.

633 Alvarez-Cuesta, M., Toimil, A., Losada, I.J., 2021a. Modelling long-term
634 shoreline evolution in highly anthropized coastal areas. part 1: Model
635 description and validation. Coastal Engineering 169. doi:10.1016/j.
636 coastaleng.2021.103960.

637 Alvarez-Cuesta, M., Toimil, A., Losada, I.J., 2021b. Modelling long-term
638 shoreline evolution in highly anthropized coastal areas. part 2: Assessing
639 the response to climate change. Coastal Engineering 168. doi:10.1016/j.
640 coastaleng.2021.103961.

641 Alvarez-Cuesta, M., Toimil, A., Losada, I.J., 2024. Which data assimila-
642 tion method to use and when: unlocking the potential of observations in
643 shoreline modelling. Environmental Research Letters 19. doi:10.1088/
644 1748-9326/ad3143.

645 Antolínez, J.A., Méndez, F.J., Anderson, D., Ruggiero, P., Kaminsky, G.M.,
646 2019. Predicting climate-driven coastlines with a simple and efficient mul-
647 tiscale model. Journal of Geophysical Research: Earth Surface 124, 1596–
648 1624. doi:10.1029/2018JF004790.

649 Bertin, S., Floc'h, F., Dantec, N.L., Jaud, M., Cancouët, R., Franzetti,
650 M., Cuq, V., Prunier, C., Ammann, J., Augereau, E., Lamarche, S., Bel-
651 leney, D., Rouan, M., David, L., Deschamps, A., Delacourt, C., Suanez,
652 S., 2022. A long-term dataset of topography and nearshore bathymetry
653 at the macrotidal pocket beach of porsmilin, france. Scientific Data 9.
654 doi:10.1038/s41597-022-01170-3.

Bertsimas, D., Tsitsiklis, J., 1993. Simulated annealing. Statistical Science 8, 10–15.

Boudière, E., Maisondieu, C., Ardhuin, F., Accensi, M., Pineau-Guillou, L., Lepesqueur, J., 2013. A suitable metocean hindcast database for the design of marine energy converters. International Journal of Marine Energy 3-4. doi:10.1016/j.ijome.2013.11.010.

Bruun, P., 1962. Sea-level rise as a cause of shore erosion. Journal of the Waterways and Harbors Division 88, 117–132. URL: https://ascelibrary.org/doi/pdf/10.1061/JWHEAU.0000252?download=true, doi:https://doi.org/10.1061/JWHEAU.000025.

Castelle, B., Bujan, S., Ferreira, S., Dodet, G., 2017. Foredune morphological changes and beach recovery from the extreme 2013/2014 winter at a high-energy sandy coast. Marine Geology 385, 41–55. URL: https://www.sciencedirect.com/science/article/pii/S0025322716303620, doi:https://doi.org/10.1016/j.margeo.2016.12.006.

Castelle, B., Bujan, S., Marieu, V., Ferreira, S., 2020. 16 years of topographic surveys of rip-channelled high-energy meso-macrotidal sandy beach. Scientific Data 7. doi:10.1038/s41597-020-00750-5.

Castelle, B., Dodet, G., Masselink, G., Scott, T., 2018a. Increased winter-mean wave height, variability, and periodicity in the northeast atlantic over 1949–2017. Geophysical Research Letters 45, 3586–3596. doi:10.1002/2017GL076884.

Castelle, B., Guillot, B., Marieu, V., Chaumillon, E., Hanquiez, V., Bujan, S., Poppeschi, C., 2018b. Spatial and temporal patterns of shoreline change of a 280-km high-energy disrupted sandy coast from 1950 to 2014: Sw france. Estuarine, Coastal and Shelf Science 200, 212–223. doi:10.1016/j.ecss.2017.11.005.

Castelle, B., Marieu, V., Bujan, S., Ferreira, S., Parisot, J.P., Capo, S., Sénéchal, N., Chouzenoux, T., 2014. Equilibrium shoreline modelling of a high-energy meso-macrotidal multiple-barred beach. Marine Geology 347, 85–94. doi:10.1016/j.margeo.2013.11.003.

Castelle, B., Marieu, V., Bujan, S., Splinter, K.D., Robinet, A., Sénéchal, N., Ferreira, S., 2015. Impact of the winter 2013-2014 series of severe western europe storms on a double-barred sandy coast: Beach and dune erosion and megacusp embayments. Geomorphology 238, 135–148. URL: http://dx.doi.org/10.1016/j.geomorph.2015.03.006, doi:10.1016/j.geomorph.2015.03.006.

Castelle, B., Masselink, G., 2023. Morphodynamics of wave-dominated beaches. Cambridge Prisms: Coastal Futures 1, e1. doi:10.1017/cft.2022.2.

Castelle, B., Masselink, G., Scott, T., Stokes, C., Konstantinou, A., Marieu, V., Bujan, S., 2021. Satellite-derived shoreline detection at a high-energy meso-macrotidal beach. Geomorphology 383. doi:10.1016/j.geomorph.2021.107707.

Castelle, B., Ritz, A., Marieu, V., Lerma, A.N., Vandenhove, M., 2022.

Primary drivers of multidecadal spatial and temporal patterns of shoreline change derived from optical satellite imagery. Geomorphology 413. doi:10.1016/j.geomorph.2022.108360.

Cooper, J.A.G., Masselink, G., Coco, G., Short, A.D., Castelle, B., Rogers, K., Anthony, E.J., Green, A.N., Kelley, J.T., Pilkey, O.H., Jackson, D.W.T., 2020. Sandy beaches can survive sea-level rise. Nature Climate Change 10, 993 – 995.

D'Anna, M., Idier, D., Castelle, B., Cozannet, G.L., Rohmer, J., Robinet, A., 2020. Impact of model free parameters and sea-level rise uncertainties on 20-years shoreline hindcast: the case of truc vert beach (sw france). Earth Surface Processes and Landforms 45, 1895–1907. doi:10.1002/esp.4854.

D'Anna, M., Idier, D., Castelle, B., Rohmer, J., Cagigal, L., Mendez, F.J., 2022. Effects of stochastic wave forcing on probabilistic equilibrium shoreline response across the 21st century including sea-level rise. Coastal Engineering 175. doi:10.1016/j.coastaleng.2022.104149.

Davidson, M.A., Splinter, K.D., Turner, I.L., 2013. A simple equilibrium model for predicting shoreline change. Coastal Engineering 73, 191–202. URL: http://dx.doi.org/10.1016/j.coastaleng.2012.11.002, doi:10.1016/j.coastaleng.2012.11.002.

Gallagher, E.L., MacMahan, J., Reniers, A., Brown, J., Thornton, E.B., 2011. Grain size variability on a rip-channeled beach. Marine Geology 287, 43 – 53. doi:10.1016/j.margeo.2011.06.010.

Ghermandi, A., Nunes, P.A., 2013. A global map of coastal recreation values: Results from a spatially explicit meta-analysis. Ecological Economics 86, 1–15. doi:10.1016/j.ecolecon.2012.11.006.

Hersbach, Bell, B., Berrisford, P., Biavati, G., Horányi, A., Sabater, J.M., Nicolas, J., Peubey, C., Radu, R., Rozum, I., Schepers, D., Simmons, A., Soci, C., Dee, D., Thépaut, J.N., 2023. Era5 hourly data on single levels from 1940 to present. Copernicus Climate Change Service (C3S) Climate Data Store (CDS) (Accessed on 16-Oct-2023). doi:10.24381/cds.adbb2d47.

Holman, R., Stanley, J., Ozkan-Haller, T., 2003. Applying video sensor networks to nearshore environment monitoring. IEEE Pervasive Computing 2, 14–21. doi:10.1109/MPRV.2003.1251165.

Ibaceta, R., Splinter, K.D., Harley, M.D., Turner, I.L., 2020. Enhanced coastal shoreline modeling using an ensemble kalman filter to include non-stationarity in future wave climates. Geophysical Research Letters 47. doi:10.1029/2020GL090724.

Ibaceta, R., Splinter, K.D., Harley, M.D., Turner, I.L., 2022. Improving multi-decadal coastal shoreline change predictions by including model parameter non-stationarity. Frontiers in Marine Science 9. doi:10.3389/fmars.2022.1012041.

Konstantinou, A., Scott, T., Masselink, G., Stokes, K., Conley, D., Castelle, B., 2023. Satellite-based shoreline detection along high-energy macroti-

dal coasts and influence of beach state. Marine Geology 462, 107082. doi:https://doi.org/10.1016/j.margeo.2023.107082.

Labarthe, C., Castelle, B., Marieu, V., Garlan, T., Bujan, S., 2023. Observation and modeling of the equilibrium slope response of a high-energy meso-macrotidal sandy beach. Journal of Marine Science and Engineering 11, 584. doi:10.3390/jmse11030584.

Laporte-Fauret, Q., Lubac, B., Castelle, B., Michalet, R., Marieu, V., Bombrun, L., Launeau, P., Giraud, M., Normandin, C., Rosebery, D., 2020. Classification of atlantic coastal sand dune vegetation using in situ, uav, and airborne hyperspectral data. Remote Sensing 12. doi:10.3390/rs12142222.

Larson, M., Kraus, N.C., 1995. Prediction of cross-shore sediment transport and temporal scales at different spatial. Marine Geology 126, 11–127.

Ludka, B.C., Guza, R.T., O'Reilly, W.C., Merrifield, M.A., Flick, R.E., Bak, A.S., Hesser, T., Bucciarelli, R., Olfe, C., Woodward, B., Boyd, W., Smith, K., Okihiro, M., Grenzeback, R., Parry, L., Boyd, G., 2019. Sixteen years of bathymetry and waves at san diego beaches. Scientific Data 6. doi:10.1038/s41597-019-0167-6.

Luijendijk, A., Hagenaars, G., Ranasinghe, R., Baart, F., Donchyts, G., Aarninkhof, S., 2018. The state of the world's beaches. Scientific Reports 8. doi:10.1038/s41598-018-24630-6.

Masselink, G., Castelle, B., Scott, T., Dodet, G., Suanez, S., Jackson, D., Floc'H, F., 2016. Extreme wave activity during 2013/2014 winter and

morphological impacts along the atlantic coast of europe. Geophysical Research Letters 43, 2135–2143. doi:10.1002/2015GL067492.

McCarroll, R., Valiente, N., Wiggins, M., Scott, T., Masselink, G., 2023. Coastal survey data for perranporth beach and start bay in southwest england (2006–2021). Scientific Data 10. doi:10.1038/s41597-023-02131-0.

Mentaschi, L., Vousdoukas, M., Garcia-Sanchez, G., Montblanc, T.F., Roland, A., Voukouvalas, E., Federico, I., Abdolali, A., Zhang, Y.J., Feyen, L., 2023. A global unstructured, coupled, high-resolution hindcast of waves and storm surges. EarthArXiv URL: https://arxiv.org/abs/2306.16337, doi:https://doi.org/10.48550/arXiv.2306.16337.

Michaud, H., Pasquet, A., Leckler, F., Baraille, R., Dalphinet, A., Aouf, L., 2016. Improvements of the new french coastal wave forecasting system and application to a wave-current interaction study. 14th International Workshop on Wave Hindcasting and Forecasting & 5th Coastal Hazard Symposium SHOM & Meteo France. URL: https://www.researchgate.net/publication/312919454, doi:10.13140/RG.2.2.13218.02243.

Montaño, J., Coco, G., Antolínez, J.A., Beuzen, T., Bryan, K.R., Cagigal, L., Castelle, B., Davidson, M.A., Goldstein, E.B., Ibaceta, R., Idier, D., Ludka, B.C., Masoud-Ansari, S., Méndez, F.J., Murray, A.B., Plant, N.G., Ratliff, K.M., Robinet, A., Rueda, A., Sénéchal, N., Simmons, J.A., Splinter, K.D., Stephens, S., Townend, I., Vitousek, S., Vos, K., 2020. Blind testing of shoreline evolution models. Scientific Reports 10. doi:10.1038/s41598-020-59018-y.

Murray, A.B., 2007. Reducing model complexity for explanation and prediction. Geomorphology 90, 178–191. doi:10.1016/j.geomorph.2006.10.020.

Ojeda, E., Ruessink, B.G., Guillen, J., 2008. Morphodynamic response of a two-barred beach to a shoreface nourishment. Coastal Engineering 55, 1185–1196. doi:10.1016/j.coastaleng.2008.05.006.

Pianca, C., Holman, R., Siegle, E., 2015. Shoreline variability from days to decades: Results of long-term video imaging. Journal of Geophysical Research: Oceans 120, 2159–2178. doi:10.1002/2014JC010329.

Pineau-Guillou, L., 2013. Projet PJ0303 : Océanographie Côtière Opérationnelle Action A030310P : CPER-PREVIMER volet 2-Etude et validation de configurations modèles physiques Département Océanographie et Dynamique des Ecosystèmes Unité Dynamiques de l'Environnement Côtier Laboratoire Physique Hydrodynamique et Sédimentaire-ODE/DYNECO/PHYSED/2013-05 version 1.0 PREVIMER Validation des modèles hydrodynamiques 2D des côtes de la Manche et de l'Atlantique. Technical Report. Ifremer. URL: https://archimer.ifremer.fr/doc/00157/26800/.

Ranasinghe, R., Turner, I.L., 2006. Shoreline response to submerged structures: A review. Coastal Engineering 53, 65–79. doi:10.1016/j.coastaleng.2005.08.003.

Robin, N., Billy, J., Castelle, B., Hesp, P., Lerma, A.N., Laporte-Fauret, Q., Marieu, V., Rosebery, D., Bujan, S., Destribats, B., Michalet, R., 2021.

150 years of foredune initiation and evolution driven by human and natural processes. Geomorphology 374. doi:10.1016/j.geomorph.2020.107516.

Robinet, A., Castelle, B., Idier, D., Cozannet, G.L., Déqué, M., Charles, E., 2016. Statistical modeling of interannual shoreline change driven by north atlantic climate variability spanning 2000–2014 in the bay of biscay. Geo-Marine Letters 36, 479–490. doi:10.1007/s00367-016-0460-8.

Robinet, A., Castelle, B., Idier, D., Harley, M.D., Splinter, K.D., 2020. Controls of local geology and cross-shore/longshore processes on embayed beach shoreline variability. Marine Geology 422. doi:10.1016/j.margeo.2020.106118.

Robinet, A., Idier, D., Castelle, B., Marieu, V., 2018. A reduced-complexity shoreline change model combining longshore and cross-shore processes: The lx-shore model. Environmental Modelling and Software 109, 1–16. doi:10.1016/j.envsoft.2018.08.010.

Senechal, N., Coco, G., Bryan, K.R., Holman, R.A., 2011. Wave runup during extreme storm conditions. Journal of Geophysical Research: Oceans 116. doi:10.1029/2010JC006819.

Small, C., Nichols, J.R., 2003. A global analysis of human settlement in coastal zones. Journal of Coastal Research 19, 584–589. URL: https://www.researchgate.net/publication/244956994, doi:10.2307/4299200.

Splinter, K.D., Turner, I.L., Davidson, M.A., 2013. How much data is enough? the importance of morphological sampling interval and dura-

tion for calibration of empirical shoreline models. Coastal Engineering 77, 14–27. doi:10.1016/j.coastaleng.2013.02.009.

Splinter, K.D., Turner, I.L., Davidson, M.A., Barnard, P., Castelle, B., Oltman-Shay, J., 2014. A generalized equilibrium model for predicting daily to interannual shoreline response. Journal of Geophysical Research: Earth Surface 119, 1936–1958. doi:10.1002/2014JF003106.

Tran, Y.H., Barthélemy, E., 2020. Combined longshore and cross-shore shoreline model for closed embayed beaches. Coastal Engineering 158. doi:10.1016/j.coastaleng.2020.103692.

Turner, I.L., Harley, M.D., Short, A.D., Simmons, J.A., Bracs, M.A., Phillips, M.S., Splinter, K.D., 2016. A multi-decade dataset of monthly beach profile surveys and inshore wave forcing at narrabeen, australia. Scientific Data 3. doi:10.1038/sdata.2016.24.

Vitousek, S., Barnard, P.L., Limber, P., Erikson, L., Cole, B., 2017. A model integrating longshore and cross-shore processes for predicting long-term shoreline response to climate change. Journal of Geophysical Research: Earth Surface 122, 782–806. doi:10.1002/2016JF004065.

Vitousek, S., Vos, K., Splinter, K.D., Erikson, L., Barnard, P.L., Survey, U.S.G., 2023. A model integrating satellite-derived shoreline observations for predicting fine-scale shoreline response to waves and sea-level rise across large coastal regions a model integrating satellite-derived shoreline observations for predicting fine-scale shoreline response to waves and sea-level rise across large coastal regions 2. Journal of Geophysical Research: Earth Sur-

face URL: https://doi.org/10.22541/essoar.167839941.16313003/v1, doi:10.22541/essoar.167839941.16313003/v1.

Vos, K., Harley, M.D., Splinter, K.D., Simmons, J.A., Turner, I.L., 2019a. Sub-annual to multi-decadal shoreline variability from publicly available satellite imagery. Coastal Engineering 150, 160–174. doi:10.1016/j.coastaleng.2019.04.004.

Vos, K., Splinter, K., Palomar-Vázquez, J., Pardo-Pascual, J., Almonacid-Caballer, J., Cabezas-Rabadán, C., Kras, E., Luijendijk, A., Calkoen, F., Almeida, L., Pais, D., Klein, A., Mao, Y., Harris, D., Castelle, B., Buscombe, D., Vitousek, S., 2023. Benchmarking satellite-derived shoreline mapping algorithms. Communications Earth and Environment 4. doi:10.1038/s43247-023-01001-2.

Vos, K., Splinter, K.D., Harley, M.D., Simmons, J.A., Turner, I.L., 2019b. Coastsat: A google earth engine-enabled python toolkit to extract shorelines from publicly available satellite imagery. Environmental Modelling and Software 122. doi:10.1016/j.envsoft.2019.104528.

Vousdoukas, M.I., Ranasinghe, R., Mentaschi, L., Plomaritis, T.A., Athanasiou, P., Luijendijk, A., Feyen, L., 2020. Sandy coastlines under threat of erosion. Nature Climate Change 10, 260–263. doi:10.1038/s41558-020-0697-0.

Warrick, J.A., Buscombe, D., Vos, K., R., B.K., Castelle, B., Cooper, A., Harley, M.D., T., J.D.W., Ludka, B., Masselink, G., Palmsten, L., R., A.A.A., Sénéchal, N., Sherwood, C.R., D., S.A., Sogut, E., D., S.K.,

Stephenson, W.J., Syvitski, J., Woodroffe, C.D., Young, A.P., submitted. Evaluating climate signals on global shoreline position : A commentary on "influence of el niño on the variability of global 2 shoreline position". EarthArXiv doi:https://doi.org/10.31223/X5W66T.

Warrick, J.A., Vos, K., Buscombe, D., Ritchie, A.C., Curtis, J.A., 2023. A large sediment accretion wave along a northern california littoral cell. Journal of Geophysical Research: Earth Surface 128, e2023JF007135. doi:https://doi.org/10.1029/2023JF007135.

Wright, L., Short, A., 1984. Morphodynamic variability of surf zones and beaches: A synthesis. Marine Geology 56, 93–118. URL: http://linkinghub.elsevier.com/retrieve/pii/0025322784900082, doi:10.1016/0025-3227(84)90008-2.

Yates, M.L., Guza, R.T., O'Reilly, W.C., 2009. Equilibrium shoreline response: Observations and modeling. Journal of Geophysical Research: Oceans 114. doi:10.1029/2009JC005359.

Satellite-derived equilibrium shoreline modelling at a high-energy meso-macrotidal beach

Highlights :

- Model calibration using uncorrected satellite-derived shoreline data.
- Simulated annealing extracts information from raw satellite derived shoreline data.
- New perspective in modelling sandy shoreline change even when lacking field data.
- Sampling frequency more critical than data quality in model calibration.

Declaration of interests

☒ The authors declare that they have no known competing financial interests or personal relationships that could have appeared to influence the work reported in this paper.

☐The authors declare the following financial interests/personal relationships which may be considered as potential competing interests: